Zeitschrift für anorganische und allgemeine Chemie

Journal of Inorganic and General Chemistry
ZAAC
Zeitschrift für anorganische und allgemeine Chemie

RESEARCH ARTICLE OPEN ACCESS

Dy_2 Schiff Base Single Molecule Magnet Forming a Halogen Bonding Network: Experiment and Theory

Jonas Braun[1,2,3] | Christian F. Pachl[1,2] | Michael Schulze[4] | Jinkui Tang[5] | Wolfgang Wernsdorfer[3,4] | Christopher E. Anson[1] | Karin Fink[2] | Annie K. Powell[1,2,3]

[1]Institute of Inorganic Chemistry, Karlsruhe Institute of Technology (KIT), Karlsruhe, Germany | [2]Institute of Nanotechnology, Karlsruhe Institute of Technology (KIT), Karlsruhe, Germany | [3]Institute for Quantum Materials and Technologies, Karlsruhe Institute of Technology (KIT), Karlsruhe, Germany | [4]Physikalisches Institut, Karlsruhe Institute of Technology (KIT), Karlsruhe, Germany | [5]School of Chemistry and Chemical Engineering, Beijing Institute of Technology, Beijing, P. R. China

Correspondence: Jonas Braun (jonas.braun2@kit.edu) | Karin Fink (karin.fink@kit.edu) | Annie K. Powell (annie.powell@kit.edu)

Received: 14 May 2026 | **Revised:** 12 June 2026 | **Accepted:** 19 June 2026

Keywords: coordination chemistry | halogen bonding | quantum chemical calculations | single molecule magnet | supramolecular chemistry

ABSTRACT

Magnetic relaxation, mediated through molecular and lattice vibrations, is recognised as the next hurdle to overcome in terms of high-performaning Single Molecule Magnets (SMMs). One strategy is to confine molecular and lattice vibrations through intra- and intermolecular interactions to modulate the phonon spectrum. Here, we report the use of halogen bonding to engineer the crystal lattice of a Dy_2 dimer $[Dy_2Cl_4(Hopch\text{-}Br)_2]\cdot CCl_4$ involving disordered lattice solvent. The strength of the resulting network has been estimated using quantum chemical calculations. The magnetic data were investigated with SQUID magnetometry, revealing antiferromagnetic interactions between the two Dy^{III} ions as well as slow relaxation of magnetisation, with the results being in excellent agreement with ab-initio calculations.

1 | Introduction

Single Molecule Magnets (SMMs) are a class of molecules which, once magnetised, can retain magnetisation after the external magnetic field is switched off [1–4]. Return to the equilibrium state is inhibited by an energy barrier, but can occur through various slow relaxation processes [5, 6]. Dy^{III} ions have long been identified as ideal candidates to produce coordination compounds exhibiting slow magnetic relaxation owing to their large magnetic anisotropy resulting in large barrier heights [7, 8]. However, in lanthanide ions like Dy^{III}, the thermal Orbach process over the top of the energy barrier is often outdone by through-barrier processes such as quantum tunnelling of magnetisation (QTM) and spin-phonon coupling-based Raman relaxation. Whereas many strategies have been established to quench QTM [9–12], the control over phonon-based relaxation remains challenging and has become a major focus of the SMM community [13–15].

Recently, Zheng et al. were able to demonstrate a novel concept using Dy^{III} coordination complexes with varying axial ligands which are more or less prone to engage in interactions with other parts of the molecule. They were able to show that these intramolecular interactions confine the respective molecular vibrations and thus modulate the phonon spectrum which can lead to an improvement in SMM performance [16].

Although long established as very influential when it comes to the magnetic behaviour of spin crossover compounds [17, 18], the role of intermolecular interactions is an aspect often overlooked when it comes to SMM properties and their relaxation

Jonas Braun and Christian F. Pachl contributed equally to this work.

Dedicated to Prof. Dr. Claus Feldmann on the occasion of his 60th birthday.

mechanisms. Thus, the motivation for the project, which led to the current manuscript, was the systematic exploration of intermolecular interactions, and their effect on magnetic relaxation. We identified halogen bonding (XB) as an ideal means to induce intermolecular interactions in SMMs. In such interactions electron density is donated from the XB-acceptor XB_A into the σ-hole of a covalently bound halogen atom, the XB-donor XB_D. Although rarely used in inorganic coordination clusters, these interactions can be tuned in strength through the choice of halogen atom and facilitate the formation of strongly bound intermolecular networks [19–23]. We have furthermore previously been able to show that the total stabilisation energy of such a network between lanthanide clusters can exceed the sum of the individual halogen bonding interactions through cooperative effects [24].

Here, we report the targeted synthesis of a Dy^{III}-based SMM with the formula $[Dy_2Cl_4(Hopch\text{-}Br)_2]\cdot CCl_4$ (**1**) (where Hopch-Br^- is the singly deprotonated form of the (*E*)-*N*'-(5-bromo-2-hydroxy-3-methoxybenzylidene)pyrazine-2-carbohydrazide ligand (H_2opch-Br)), forming a halogen-bonded network, including the participation of disordered lattice CCl_4. A quantum chemical study of the crystal structure helps rationalise the strength and directionality of the supramolecular halogen bonding network of **1,** involving the disordered CCl_4.

2 | Results and Discussion

2.1 | Synthesis

In order to induce halogen bonding in a Dy^{III}-based SMM, a ligand system was chosen that is known to form different structural motifs of various nuclearity, which all exhibit slow relaxation of magnetisation [25–28]. The H_2opch ligand system was extended to carry a Br atom in the 5-position of the *o*-vanillin unit of the Schiff base, introducing a potential halogen bond donor and/or acceptor into the system (Scheme 1). The potential of this H_2opch-Br ligand to form halogen bonds was previously shown by some of us in an Er_6 cluster, which forms an unusual 3D network through intermolecular halogen bonding [24]. To further enhance the opportunities for intermolecular halogen bonding, two additional measures were taken: 1) $DyCl_3\cdot 6H_2O$ was chosen as the lanthanide source, and 2) halogen-containing additives were added, as these are often shown to enhance halogen bonding in organic crystals [22, 29]. Several additives were tested during the work on this project, including 1,4-diiodobenzene, CBr_4, and CCl_4, for example. Of these, only the reaction mixture containing CCl_4 led to the formation of a crystalline Dy-compound. The reason for this is probably that using a MeOH-CCl_4 solvent mixture led to a rather nonpolar mixture where CCl_4 was essentially acting as an antisolvent for the Dy-cluster, aiding crystallisation, whereas the other two solid additives were added to a much more polar reaction solution using only MeOH as solvent. The combination of $DyCl_3\cdot 6H_2O$, H_2opch-Br, and Et_3N as base in a 7:3 MeOH/CCl_4 solvent mixture was loaded into a Wheaton vial and heated to 90°C in an oven under solvothermal conditions, resulting in a low yield of cuboid orange crystals of **1** (details on the exact amounts can be found in the Experimental Section).

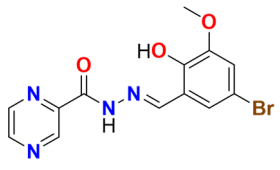

SCHEME 1 | Structure of the keto tautomer of H_2opch-Br.

2.2 | Crystallography

The dimeric complex $[Dy_2Cl_4(Hopch\text{-}Br)_2]\cdot CCl_4$ (**1**) crystallises in the tetragonal space group P4/n (origin choice 2 on $\bar{1}$) with $Z=4$. Within the centrosymmetric Dy_2 complex, Figure 1a, each $(Hopch\text{-}Br)^-$ ligand chelates Dy(1) via its phenoxo oxygen O(1) and by N(1) and O(3) of the carboxyhydrazone group, while O(1) and the methoxy oxygen O(2) coordinate to Dy(1′) at 1-x, 1-y, 1-z. Dy(1) and Dy(1′) are thus doubly-bridged by O(1) and O(1′), with Dy(1)-O(1) and O(1)-Dy(1′) 2.329(4) and 2.337(3) Å, respectively, and Dy(1)-O(1)-Dy(1′) 103.76(14)°. This results in a Dy(1)···Dy(1′) distance of 3.6708(5) Å. The carboxyhydrazone functionality of the ligand is clearly in the still-protonated keto tautomer, with C(9)-O(3) at 1.251(7) Å consistent with a double bond, while N(2) remains protonated with the N-H forming a hydrogen bond to N(4) of the dimer molecule at -y+½, x, z. The ligand is thus a monoanion, with only the phenolic oxygen being deprotonated. The $[Dy_2(Hopch\text{-}Br)_2]^{4+}$ unit is almost planar, with the O(3) and O(3′) showing the largest displacements out of the

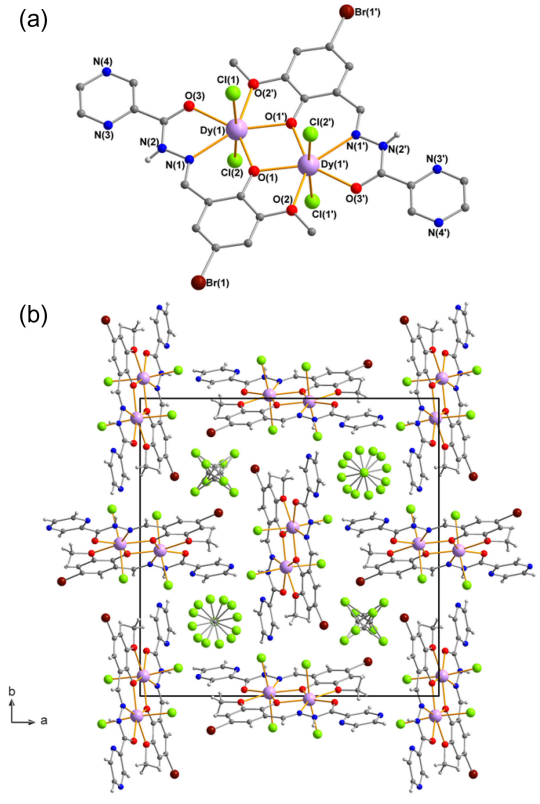

FIGURE 1 | (a) Molecular structure of the $[Dy_2Cl_4(Hopch\text{-}Br)_2]$ (organic H-atoms omitted for clarity) in **1**, and (b) a packing diagram for **1** viewed along the *c*-axis showing the disordered CCl_4 lattice solvent molecules.

mean plane, 0.218 Å, while the mean displacement of the atoms from the plane is only 0.033 Å. The approximately pentagonal-bipyramidal coordination environment of Dy(1) (the Continuous Shape Measure [30], giving a value of 0.425 for this coordination geometry) is completed by two chloride ligands with Dy(1)-Cl(1) and Dy(1)-Cl(2) 2.5895(16) and 2.5815(17) Å, respectively. The two Dy—Cl bonds are not quite colinear, with Cl1(-Dy)1-Cl(2) 171.94(6)°. This results from the two chlorides over the same face of the $[Dy_2(Hopch\text{-}Br)_2]^{4+}$ unit slightly bending away from each other, such that the Cl(1)···Cl(2′) distance is 4.021(3) Å, 0.35 Å longer than the Dy···Dy distance.

Whereas the Dy_2 complex is situated on an inversion centre (Wyckoff site 4e, $\bar{1}$, at ½, ½, ½), the CCl_4 molecules occupy higher-symmetry sites in the crystal lattice. The CCl_4 molecule containing C(21) occupies the Wyckoff site 2c, at ¼, ¼, z, with the C(21)—Cl(3) bond lying on this fourfold axis. The remaining three chlorine atoms of the molecule are disordered according to the fourfold symmetry, with twelve quarter-occupancy chlorines arranged in a ring about the axis. The CCl_4 molecule centred on C(22) occupies the Wyckoff site 2b, $\bar{4}$, at ¼, ¾, ½. Although the CCl_4 molecular geometry is compatible with this $\bar{4}$ site symmetry, this molecule is nonetheless also disordered, since C(22) is displaced from this special position by 0.441 Å to a general site meaning that the molecule is disordered over four closely spaced sites. Given that the multiplicities of the two CCl_4 sites are both half that of the Dy_2 site, there is therefore in total one CCl_4 per Dy_2 complex. The arrangement of the disordered lattice CCl_4 molecules relative to the dimeric complexes is clearly seen in a packing diagram viewed down the c-axis (Figure 1b).

3 | Halogen Bonding Network and Quantum Chemical Calculations

In total, there are 5 distinct short intermolecular contacts that were investigated for possible halogen bonding (see Table 1): Cl(1) forms a short contact with Cl(6) which is part of the CCl_4 at the $\bar{4}$ site. This Cl is connected to two disordered C22 positions; one in the asymmetric unit and one at ½+y, 1-x, 1-z. These two contacts will in the following be referred to $S_4(1)$ and $S_4(2)$. Cl(2) forms two short contacts to Cl(4), which belongs to the CCl_4 at the 4-axis. In particular, one contact is to Cl(4A) in the same asymmetric unit and to Cl(4C) belonging to y, ½-x, z. These two contacts will now be referred to as $C_4(1)$ and $C_4(2)$. Given these symmetries this means that every CCl_4 molecule is connected to two different Dy_2 molecules. Finally, the Br atom forms a short contact to the phenyl ring (C5), abbreviated as Br-π at the position 1-y, ½+x, -z.

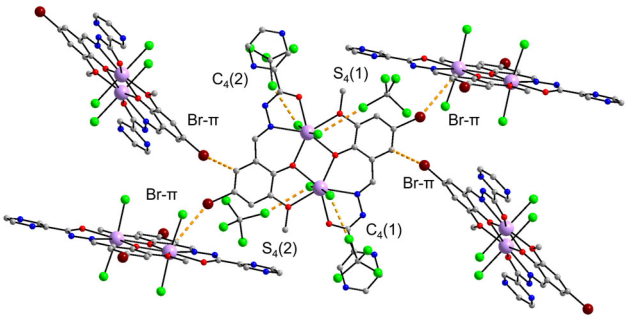

FIGURE 2 | Halogen bonds connecting a Dy_2 dimer with neighbouring complexes and lattice molecules.

Therefore, each Dy_2-unit is involved in six halogen bonding interactions (see Figure 2). This unit acts as XB_D through two Br-atoms, as XB_A for two Br-π interactions. The terminal chloride ligands on each Dy_2 unit act as XB_A for (on average) two halogen contacts to the disordered CCl_4 lattice solvents (see also Figure S2).

The Br-π interactions, together with the N—H hydrogen bond to N(4) at -y+½, x, z, form a 3-dimensional supramolecular structure with two types of cavities at the Wyckoff sites 2b and 2c. These are then filled with the CCl_4 molecules (Figures S3 and S4). A list of the investigated contacts is provided in Table 1. All contacts are shorter than the sum of the van der Waals radii (Br–C = 3.55 Å, Cl–Cl = 3.50 Å) [31].

In order to estimate the stabilisation energy of the lattice through these intermolecular halogen contacts, we performed a series of DFT calculations to compute the interaction energy E_{int} between the interacting fragments. We used three benchmarked [32–34] functionals, M06-2X [35], PBE0 [36], and CAM-B3LYP [37]. These were chosen to cover hybrid functionals with low and high exact exchange and a range-separated functional. Furthermore, we used D4-dispersion correction [38, 39] and corrected for the basis set superposition error using the counterpoise correction [40]. All calculations were performed using TURBOMOLE 7.8 [41, 42]. A detailed description of the calculations performed can be found in the Supporting Information. The obtained interaction energies and properties of the bond critical points [43] are summarised in Table 2.

We note that interactions $C_4(1)$, $C_4(2)$, and $S_4(2)$ involving CCl_4 are of a similar strength between −24 and −27 kJ/mol. Interaction $S_4(1)$ appears to be slightly stronger with values between −28 and −30 kJ/mol. Furthermore, the Br-π interaction (with two of them per complex) seems to be about half as stable between −12

TABLE 1 | List of short halogen contacts in compound **1**.

Interaction	Involved atoms	XB_A-XB_D distance, Å	C-XB_D-XB_A angle, °
$C_4(1)$	Cl(2)-Cl(4A)	3.11(3)	159.1(12)
$C_4(2)$	Cl(2)-Cl(4C) (y, ½-x, z)	3.17(3)	153.5(14)
$S_4(1)$	Cl(1)-Cl(6)	3.388(7)	178.7(5)
$S_4(2)$	Cl(1)-Cl(6)*	3.388(7)	158.8(5)
Br-π	Br(1)-C(5) (1-y, ½+x, -z)	3.268(6)	154.8(2)

Note: *Cl(6) is bonded to C(22) from the asymmetric unit ½+y, 1-x, 1-z.

TABLE 2 | Calculated interaction energies E_{int} for the three functionals tested in kJ/mol and density (ρ) and Laplacian (∇^2) at the bond critical points (BCP) calculated using the M06-2X functional.

Interaction	E_{int} (M06-2X)	E_{int} (PBE0)	E_{int} (CAM-B3LYP)	ρ (BCP)	∇^2 (BCP)
$C_4(1)$	−24.05	−25.97	−25.97	0.0142	0.0488
$C_4(2)$	−23.62	−27.21	−27.33	0.0136	0.0472
$S_4(1)$	−27.80	−29.21	−29.95	0.0082	0.0274
$S_4(2)$	−24.50	−26.14	−26.71	0.0088	0.0271
Br-π	−12.49	−13.13	−12.91	0.0109	0.0349

and −13 kJ/mol. All interactions show a positive Laplacian at the BCP indicating the interaction is not of covalent character. The strongest interaction is the only one with a C-XB_D-XB_A angle close to 180° albeit not with the shortest contact. To further rationalise the differences between the interactions, we performed an Energy Decomposition Analysis (EDA) [44] using the PBE0 functional as shown in Figure 3.

The interactions involving CCl_4 show very similar energy contributions. There are no apparent correlations to the structural parameters, as expected, considering the very similar interaction energies. The Br-π interaction is about half as strong as the other interactions, with essentially the same energy contributions. We then computed the Electron Localisation Function (ELF) and the molecular electrostatic potential (MEP) which confirm that these interactions are indeed involving the σ-hole at the XB_D (Figures S5–S10) and follow the expected interaction pattern for halogen bonding. Thus, we conclude that all five interactions can be categorised as halogen bonds. This results in an average stabilisation between 75 and 81 kJ/mol per Dy_2 unit.

4 | Magnetic Properties

To gain insights into the magnetic properties of **1,** we performed a series of ab-initio calculations using our in-house developed Complete Active Space Spin Orbit Configuration Interaction (CASOCI) program [45]. We tested two model structures, one where four CCl_4 molecules are bonded to the Dy_2 unit and one where only the complex was considered. Details of the calculations can be found in the Supporting Information. The energies of the eight Kramers' Doublets (KDs) of the $^6H_{15/2}$ ground state multiplet, their diagonal g-tensor components, m_J-compositions, and Extended Stevens Operator Equivalents (ESOs) are provided in Tables S2–S6. The inclusion of additional CCl_4 molecules did not have a significant influence on the ground state electronic properties. Thus, we will continue to discuss the model only considering the complex. We find that the ground state KD is highly axial with $g_z = 19.86$, $g_x = 0.002$, and $g_y = 0.003$. The first excited KD is at 379.7 K and thus well separated from the ground state.

A MAGELLAN analysis [46] of the compound shows that the two principal magnetic axes are parallel (conforming with the centrosymmetric molecular structure) and essentially perpendicular to the Dy–Dy vector with an angle of 85.3° to this vector (see Figure 4). Given that this value is larger than the magic angle (54.74°) this means that the dipolar coupling between the two Dy^{III} ions is antiferromagnetic [47]. Furthermore, from literature precedent in such dimers [28, 48, 49] and the inter-Dy distance of 3.6708(5) Å, keeping in mind the $J_{dip} \propto 1/r^3$ relation of the dipolar coupling strength, it can be expected that the antiferromagnetic dipolar interaction is the dominant magnetic interaction in compound **1**. This is corroborated by our computational analysis suggesting almost identical magnetic main axes and an antiferromagnetic coupling between the ground state KDs of $-1.70\,cm^{-1}$ (for a Spin Hamiltonian $\hat{H}_{dip} = -2J\hat{S}_1\hat{S}_2$ for two pseudospins ½).

Experimentally, the magnetic properties of **1** were investigated using dc and ac SQUID as well as microSQUID magnetometry. The $\chi_M T$ versus T curve in Figure 5, left, was recorded under a

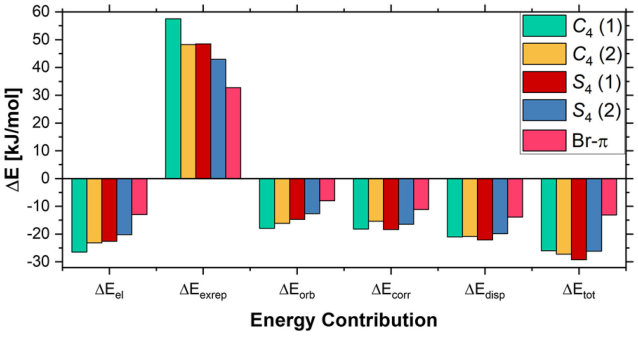

FIGURE 3 | Energy Decomposition Analysis (EDA) for the five interactions investigated. These include electrostatic (E_{el}), exchange-repulsion (E_{exrep}), orbital relaxation (E_{orb}), correlation (E_{corr}) and dispersion (E_{disp}) contributions. The sum of these contributions is given as E_{tot}.

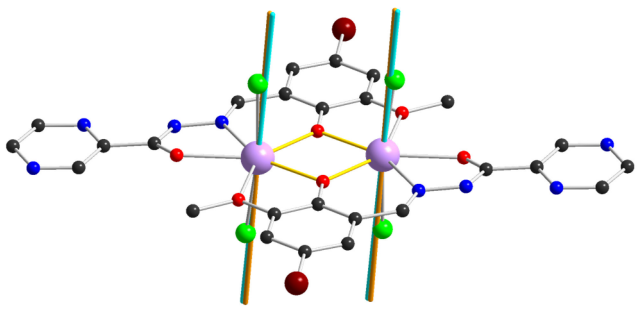

FIGURE 4 | MAGELLAN (blue) and CASOCI (orange) analysis of compound **1** revealing the Dy-axes to be essentially perpendicular to the Dy–Dy vector [45, 46].

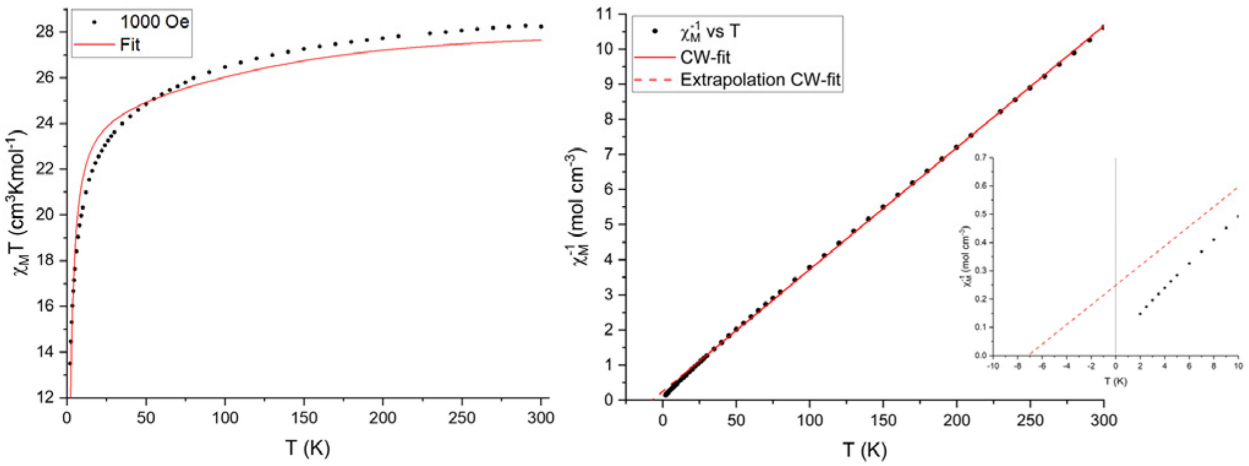

FIGURE 5 | $\chi_M T$ versus T plot of **1** under an applied dc magnetic field of 1000 Oe as well as a fit of the data (left). Curie–Weiss plot confirming the presence of dominant antiferromagnetic coupling between the Dy^{III} ions (right).

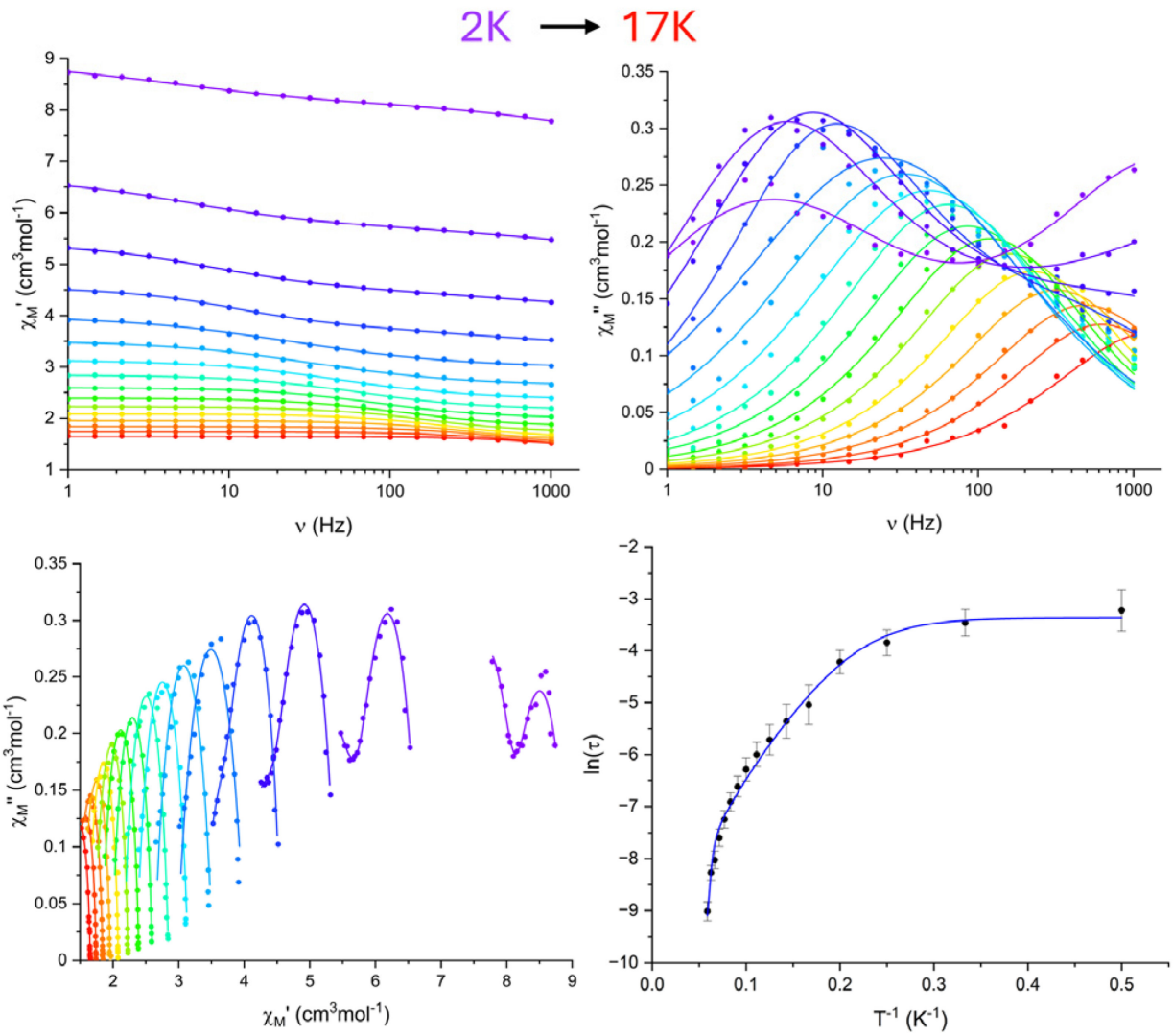

FIGURE 6 | Frequency dependence of in- and out-of-phase ac susceptibility of 1 under zero applied magnetic dc field (top, left, and right, respectively). Cole–Cole plots revealing the presence of multiple relaxation processes, in particular at low temperatures (bottom, left). Temperature dependence of the extracted relaxation times fitted using a multicomponent equation.

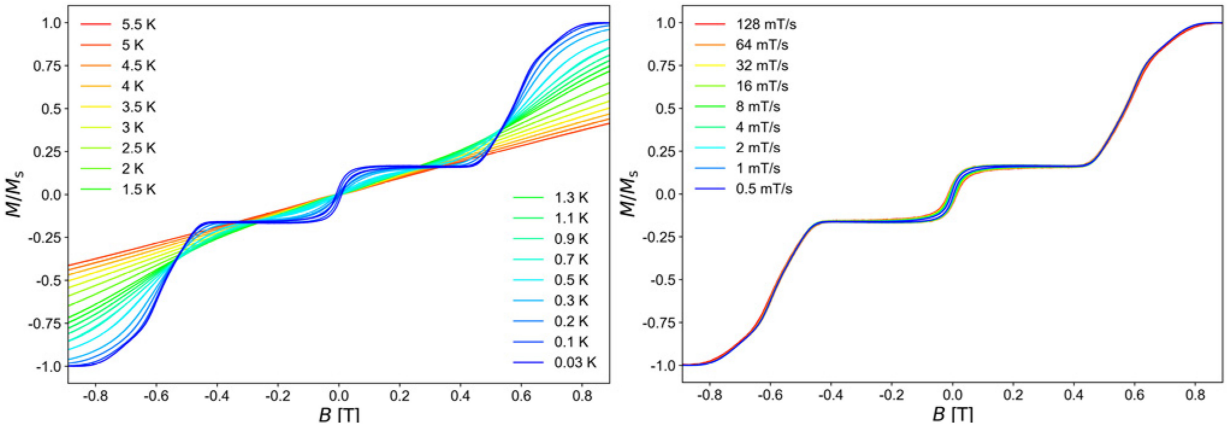

FIGURE 7 | Temperature (left) and field-sweep-rate dependent (right) microSQUID measurements of **1** revealing an open hysteresis only at very low temperatures.

magnetic dc field of 1000 Oe. The $\chi_M T$ value of 28.24 $cm^3 Kmol^{-1}$ at 300 K is in excellent agreement with the expected value of two uncoupled Dy^{III} ions (28.34 $cm^3 Kmol^{-1}$). On lowering the temperature, a gradual decrease is observed down to ca. 30 K, below which $\chi_M T$ decreases steeply, reaching a value of 13.51 $cm^3 Kmol^{-1}$ at 2 K. We can fit the observed decrease of $\chi_M T$ over the whole observed temperature region using the computed ESOs and two pseudospins 15/2. We obtain a fitted g-value of 1.326 ± 0.001 which is very close to the ideal 4/3. The fitted J_{ex} is −0.0082 ± 0.0001 cm^{-1}. Rescaling this value to a pseudospin ½, this is −1.84 ± 0.02 cm^{-1} and therefore in excellent agreement with the calculations presented above. The presence of the antiferromagnetic coupling could be further confirmed using the Curie–Weiss law to fit the χ_M^{-1} versus T data, which resulted in a Curie constant C of 28.64(7) $cm^3 Kmol^{-1}$ and a Weiss constant θ of −7.1(3) K (see Figure 5, right).

The dynamic behaviour of **1** was investigated using ac magnetometry. Under zero applied dc magnetic field, maxima in the out-of-phase component of the magnetic susceptibility were observed, confirming the presence of slow magnetic relaxation as expected from the highly axial ground state and significant energy separation of the ground and first excited KDs resulting from four axial Cl^- ligands and the coordination environment close to pentagonal bipyramidal [50, 51]. At low temperatures (ca. 2–5 K), it becomes obvious that at higher frequencies (faster relaxation) there is a second process which is not captured within the frequency window of the measurement as indicated by the upturn of χ_M'' (Figure 6, top right) and the shape of the Cole–Cole plots (see Figure 6, bottom left). This second set of maxima complicates the fitting of the data using a generalised Debye model. In order to disentangle the different processes for the lowest temperatures, a double Debye model was used, whereas the curves above 5 K were fitted using a single Debye model. The temperature dependence of the extracted τ values (τ_1 for the four lowest temperatures and τ_{single} for all temperatures above 5 K) was then fitted using the following equation

$$\tau^{-1} = B + V_a * \frac{exp\left(\frac{\omega_a}{k_B T}\right)}{\left(exp\left(\frac{\omega_a}{k_B T}\right) - 1\right)^2} + \tau_0^{-1} * exp\left(-\frac{U_{eff}}{k_B T}\right)$$

where B is the quantum tunnelling parameter, V_a and ω_a describe Raman relaxation, and τ_0 and U_{eff} the Orbach process. The temperature dependence of the relaxation times can be fitted using a range of thermal energy barrier values U_{eff} including the energy of the first excited KD obtained from ab-initio calculations of 379.7 K. This leads to the following fitting parameters keeping U_{eff} fixed to the calculated value: B = 28.9 s^{-1} ± 3.4 s^{-1}, V_a = 6803 s^{-1} ± 1832 s^{-1}, ω_a = 25.5 K ± 2.2 K, τ_0 = $3.1 \cdot 10^{-14}$ s ± $6.5 \cdot 10^{-15}$ s, and U_{eff} = 379.7 K. The best fitting, letting all parameters converge freely, are given in the Supporting Information (Table S1 and Figure S12). This suggests that although the Orbach barrier is significant, under-barrier processes such as Raman and quantum tunnelling of magnetisation dominate the dynamic behaviour at zero field.

This is corroborated by the microSQUID measurements which reveal an extremely narrow opening of magnetic hysteresis at temperatures below 0.1 K (see Figure 7).

5 | Conclusions

Halogen bonding in inorganic coordination clusters is a rare tool to engineer the crystal lattice. We have successfully synthesised a Dy_2 SMM which employs these interactions to form a 3D supramolecular network through the disordered CCl_4 lattice solvent. The strength of the halogen bonding network was investigated using quantum chemical calculations, which give a stabilisation energy between 75 and 81 kJ/mol per Dy_2 unit.

The magnetic properties of $[Dy_2Cl_4(Hopch\text{-}Br)_2]\cdot CCl_4$ (**1**) were investigated both experimentally and computationally. The analysis revealed an antiferromagnetic dipolar coupling between the Dy^{III} ions as well as slow magnetic relaxation between 2 and 17 K under zero applied magnetic dc field.

In order to gauge whether the halogen bonding indeed has an influence on the spin-phonon coupling-based relaxation mechanisms within such SMMs, comparison with related coordination clusters and further engineering of the crystal lattice network is crucial. This provides a roadmap for future investigations aiming to control phonon-based relaxation.

6 | Experimental Section

6.1 | Synthesis

All chemicals were obtained from commercial sources and used without further purification, other than the H_2opch-Br ligand, which was prepared using the procedure reported in a previous publication by some of us [24]. All syntheses were performed in air.

6.2 | $[Dy_2Cl_4(Hopch\text{-}Br)_2]\cdot CCl_4$ (1)

H_2opch-Br (52.5 mg, 0.15 mmol, 1.0 eq.) and $DyCl_3\cdot 6H_2O$ (56.5 mg, 0.15 mmol, 1.0 eq.) were weighed into a Wheaton vial before the addition of 3 ml CCl_4, 7 ml, MeOH, and Et_3N (104 µl, 0.750 mmol, 5.00 eq.). The vial was placed into an oven at 90°C for 1 day before being left to cool down to RT. The product was obtained as orange cuboid crystals in a yield of 15.1 mg (15%).

C/H/N (%): Calculated: $C = 24.55$, $H = 1.53$, $N = 8.48$; Found: $C = 24.16$, $H = 1.59$, $N = 8.83$

6.3 | Crystallography

Data were collected from a single crystal of **1** using a Stoe StadiVari diffractometer equipped with a MetalJet D2 liquid Ga source. Data were corrected for absorption and polarisation. The structure was solved by direct methods using intrinsic phasing (SHELXT [52]) and refined using full-matrix least-squares on F_o^2 (SHELXL-2019-3 [53]) within the Olex2–1.5 platform [54]. All non-H atoms were assigned anisotropic thermal parameters. Organic H-atoms were placed in calculated positions; the N-H H-atom on N(2) was refined. Both the independent lattice CCl_4 molecules are disordered over special positions. The fourfold rotational site symmetry of the molecule containing C(21) enforces disorder of three of the choline atoms, which were refined as twelve quarter-occupancy Cl-atoms arranged in a ring. The molecule containing C(22) occupies a site of $\bar{4}$ site symmetry, the carbon is displaced from this site, again resulting in fourfold disorder. In both cases, the partial atoms could be refined anisotropically without restraints; it was only necessary to apply similarity restraints to C-Cl distances.

Crystal data for **1**: $C_{27}H_{20}Br_2Cl_8Dy_2N_8O_6$, 1320.93 g mol^{-1}, tetragonal, $P4/n$, $a = 20.9056(4)$, $c = 9.1595(2)$ Å, $V = 4003.11(18)$ Å^3, $Z = 4$, T = 180(2) K, $\rho_{calc} = 2.192$ g cm^{-3}, $F(000) = 2496$, $\lambda = 1.34143$ Å, μ(Ga-$K\alpha$) = 24.286 mm^{-1}; yellow block crystal 0.12 × 0.09 × 0.05 mm, 12394 data, 4746 unique ($R_{int} = 0.0340$), 281 parameters, 13 restraints, final $wR_2 = 0.1483$, $S = 1.125$ (all data), R_1 3824 data with $I > 2\sigma(I)) = 0.0490$, largest peak/hole in final difference map + 1.74/−1.63 eÅ^{-3}.

6.4 | SQUID Magnetometry

SQUID measurements were performed on a randomly oriented powder sample of **1** immobilised in eicosane using an MPMS-XL-7 magnetometer from Quantum Design.

6.5 | Quantum Chemical Calculations

All quantum chemical calculations were performed using TURBOMOLE [42] and an in-house developed CASOCI program [45]. More detailed information can be found in the Supporting Information.

Author Contributions

Jonas Braun: synthesis and characterisation, magnetic SQUID measurements and analysis, writing of original draft, review and editing. **Christian F. Pachl**: quantum chemical calculations, writing of original draft, review and editing. **Michael Schulze**: microSQUID measurements and analysis. **Jinkui Tang**: magnetic SQUID measurements and analysis. **Wolfgang Wernsdorfer**: microSQUID measurements and analysis. **Christopher E. Anson**: crystallography, writing of original draft, review and editing. **Karin Fink**: quantum chemical calculations, review and editing, funding acquisition, supervision. **Annie K. Powell**: review and editing, funding acquisition, supervision.

Acknowledgments

The authors acknowledge funding provided by the POF MSE by the Helmholtz Foundation; CFP, JB, WW, CEA, KF and AKP thank the German Research Council (DFG) for funding through the CRC 1573 "4f for Future".

Open Access funding enabled and organized by Projekt DEAL.

Funding

This study was supported by Deutsche Forschungsgemeinschaft (CRC 1573 "4f for Future"), Helmholtz Association (POF MSE).

Conflicts of Interest

The authors declare no conflicts of interest.

Data Availability Statement

Full crystallographic data and details of the structural determination for the structure in this paper have been deposited with the Cambridge Crystallographic Data Centre as supplementary publication no. CCDC 2552026. Copies of the data can be obtained, free of charge, from https://www.ccdc.cam.ac.uk/structures/. All other data are available from the KITopen repository under the following https://doi.org/10.35097/72jwcpvjk7z59dy1.

References

1. R. Sessoli, D. Gatteschi, A. Caneschi, and M. A. Novak, "Magnetic Bistability in a Metal-Ion Cluster," *Nature* 365 (1993): 141–143.

2. F.-S. Guo, B. M. Day, Y. C. Chen, M.-L. Tong, A. Mansikkamäki, and R. A. Layfield, "Magnetic Hysteresis up to 80 kelvin in a Dysprosium Metallocene Single-Molecule Magnet," *Science* 362 (2018): 1400–1403.

3. C. A. Gould, R. K. McClain, D. Reta, et al., "Ultrahard Magnetism from Mixed-Valence Dilanthanide Complexes with Metal-Metal Bonding," *Science* 375 (2022): 198–202.

4. J. Emerson-King, G. K. Gransbury, B. E. Atkinson, et al., "Soft Magnetic Hysteresis in a Dysprosium Amide–alkene Complex up to 100 kelvin," *Nature* 643 (2025): 125–129.

5. S. T. Liddle and J. van Slageren, "Improving f-Element Single Molecule Magnets," *Chemical Society Reviews* 44 (2015): 6655–6669.

6. C. E. Jackson, I. P. Moseley, R. Martinez, S. Sung, and J. M. Zadrozny, "A Reaction-Coordinate Perspective of Magnetic Relaxation," *Chemical Society Reviews* 50 (2021): 6684–6699.

7. D. Gatteschi, "Anisotropic Dysprosium," *Nature Chemistry* 3 (2011): 830.

8. J. D. Rinehart and J. R. Long, "Exploiting Single-Ion Anisotropy in the Design of f-Element Single-Molecule Magnets," *Chemical Science* 2 (2011): 2078–2085.

9. S. K. Langley, D. P. Wielechowski, V. Vieru, et al., "A $\{Cr^{III}_2 Dy^{III}_2\}$ Single-Molecule Magnet: Enhancing the Blocking Temperature through 3d Magnetic Exchange," *Angewandte Chemie International Edition* 52 (2013): 12014–12019.

10. A. Swain, T. Sharma, and G. Rajaraman, "Strategies to Quench Quantum Tunneling of Magnetization in Lanthanide Single Molecule Magnets," *Chemical Communications* 59 (2023): 3206–3228.

11. A. B. Carter, J. Braun, T. Bodenstein, et al., "Using a Radical Straitjacket to Enforce an Ultrashort Dy–Dy Distance and Thus Enhance Dipolar Interactions in a Dy^{III}_2 Dimer," *Inorganic Chemistry* 64 (2025): 25036–25043.

12. P. B. Jin, Q. C. Luo, and Y. Z. Zheng, "Regulating Lanthanide Single-Molecule Magnets with Coordination Geometry and Organometallic Chemistry," *Accounts of Chemical Research* 59 (2026): 221–233.

13. M. Briganti, F. Santanni, L. Tesi, F. Totti, R. Sessoli, and A. Lunghi, "A Complete *Ab Initio* View of Orbach and Raman Spin–Lattice Relaxation in a Dysprosium Coordination Compound," *Journal of the American Chemical Society* 143 (2021): 13633–13645.

14. S. Mondal and A. Lunghi, "Unraveling the Contributions to Spin–Lattice Relaxation in Kramers Single-Molecule Magnets," *Journal of the American Chemical Society* 144 (2022): 22965–22975.

15. R. F. Pfleger, M. Briganti, N. Bonde, et al., "Dinuclear Dysprosium Compounds: The Importance of Rigid Bridges," *Chemistry – A European Journal* 31 (2025): e202403002.

16. Q. C. Luo, L. A. Mariano, W. J. Xu, et al., "Supramolecular Interactions Modulate Raman Relaxation in D_{5h} Symmetric Dy(III) Single-Molecule Magnets Opening the Magnetic Hysteresis up to 50 K," *Journal of the American Chemical Society* 148 (2026): 17408–17419.

17. R. Busch, A. B. Carter, K. F. Konidaris, et al., "The First Use of a ReX_5 Synthon to Modulate Fe^{III} Spin Crossover via Supramolecular Halogen···Halogen Interactions," *Chemistry – A European Journal* 26 (2020): 11835–11840.

18. O. Markin, I. Gudyma, and K. Boukheddaden, "Richness of the Nature of Intermolecular Interactions in Spin-Crossover Materials and Its Implications," *Physical Review B* 112 (2025): 104431.

19. P. Politzer, P. Lane, M. C. Concha, Y. Ma, and J. S. Murray, "An Overview of Halogen Bonding," *Journal of Molecular Modeling* 13 (2007): 305–311.

20. P. Metrangolo, F. Meyer, T. Pilati, G. Resnati, and G. Terraneo, "Halogen Bonding in Supramolecular Chemistry," *Angewandte Chemie International Edition* 47 (2008): 6114–6127.

21. A. Priimagi, G. Cavallo, P. Metrangolo, and G. Resnati, "The Halogen Bond in the Design of Functional Supramolecular Materials: Recent Advances," *Accounts of Chemical Research* 46 (2013): 2686–2695.

22. G. Cavallo, P. Metrangolo, R. Milani, et al., "The Halogen Bond," *Chemical Reviews* 116 (2016): 2478–2601.

23. M. Atzori, F. Artizzu, E. Sessini, et al., "Halogen-Bonding in a New Family of Tris(haloanilato)metallate(Iii) Magnetic Molecular Building Blocks," *Dalton Transactions* 43 (2014): 7006–7019.

24. J. Braun, C. Pachl, O. Fuhr, et al., "An Unexpected Tetragonal Network of Seven-Connected Er_6 Clusters Stabilized by Multiple Halogen Bonds through Cooperative Effects," *Crystal Growth & Design* 25 (2025): 6593–6603.

25. H. Tian, M. Wang, L. Zhao, et al., "A Discrete Dysprosium Trigonal Prism Showing Single-Molecule Magnet Behaviour," *Chemistry – A European Journal* 18 (2012): 442–445.

26. H. Tian, L. Zhao, Y. N. Guo, Y. Guo, J. Tang, and Z. Liu, "Quadruple-CO_3^{2-} Bridged Octanuclear Dysprosium(Iii) Compound Showing Single-Molecule Magnet Behaviour," *Chemical Communications* 48 (2012): 708–710.

27. H. Tian, L. Zhao, H. Lin, J. Tang, and G. Li, "Butterfly-Shaped Pentanuclear Dysprosium Single-Molecule Magnets," *Chemistry – A European Journal* 19 (2013): 13235–13241.

28. H. Tian, L. Ungur, L. Zhao, S. Ding, J. Tang, and L. F. Chibotaru, "Exchange Interactions Switch Tunneling: A Comparative Experimental and Theoretical Study on Relaxation Dynamics by Targeted Metal Ion Replacement," *Chemistry – A European Journal* 24 (2018): 9928–9939.

29. C. B. Aakeroy, M. Baldrighi, J. Desper, P. Metrangolo, and G. Resnati, "Supramolecular Hierarchy among Halogen-Bond Donors," *Chemistry – A European Journal* 19 (2013): 16240–16247.

30. M. Pinsky and D. Avnir, "Continuous Symmetry Measures. 5. The Classical Polyhedra," *Inorganic Chemistry* 37 (1998): 5575–5582.

31. A. Bondi, "Van der Waals Volumes and Radii," *The Journal of Physical Chemistry* 68 (1964): 441–451.

32. S. Kozuch, and J. M. L. Martin, "Halogen Bonds: Benchmarks and Theoretical Analysis," *Journal of Chemical Theory and Computation* 9 (2013): 1918–1931.

33. A. Siiskonen and A. Priimagi, "Benchmarking DFT Methods with Small Basis Sets for the Calculation of Halogen-Bond Strengths," *Journal of Molecular Modeling* 23 (2017): 50.

34. L. N. Anderson, F. W. Aquino, A. E. Raeber, X. Chen, and B. M. Wong, "Halogen Bonding Interactions: Revised Benchmarks and a New Assessment of Exchange Vs Dispersion," *Journal of Chemical Theory and Computation* 14 (2018): 180–190.

35. Y. Zhao and D. G. Truhlar, "The M06 Suite of Density Functionals for Main Group Thermochemistry, Thermochemical Kinetics, Noncovalent Interactions, Excited States, and Transition Elements: Two New Functionals and Systematic Testing of Four M06-Class Functionals and 12 other Functionals," *Theoretical Chemistry Accounts* 120 (2008): 215–241.

36. J. P. Perdew, M. Ernzerhof, and K. Burke, "Rationale for Mixing Exact Exchange with Density Functional Approximations," *The Journal of Chemical Physics* 105 (1996): 9982–9985.

37. T. Yanai, D. P. Tew, and N. C. Handy, "A New Hybrid Exchange–correlation Functional Using the Coulomb-Attenuating Method (CAM-B3LYP)," *Chemical Physics Letters* 393 (2004): 51–57.

38. E. Caldeweyher, C. Bannwarth, and S. Grimme, "Extension of the D3 Dispersion Coefficient Model," *The Journal of Chemical Physics* 147 (2017): 034112.

39. E. Caldeweyher, S. Ehlert, A. Hansen, et al., "A Generally Applicable Atomic-Charge Dependent London Dispersion Correction," *The Journal of Chemical Physics* 150 (2019): 154122.

40. S. F. Boys and F. Bernardi, "The Calculation of Small Molecular Interactions by the Differences of Separate Total Energies. Some Procedures with Reduced Errors," *Molecular Physics* 19 (2006): 553–566.

41. F. Weigend, "A Fully Direct RI-HF Algorithm: Implementation, Optimised Auxiliary Basis Sets, Demonstration of Accuracy and Efficiency," *Physical Chemistry Chemical Physics* 4 (2002): 4285–4291.

42. , TURBOMOLE V7.8, a development of University of Karlsruhe and Forschungszentrum Karlsruhe GmbH, TURBOMOLE GmbH, https://www.turbomole.org, 2023.

43. R. F. W. Bader and H. Essén, "The Characterization of Atomic Interactions," *The Journal of Chemical Physics* 80 (1984): 1943–1960.

44. P. Su and H. Li, "Energy Decomposition Analysis of Covalent Bonds and Intermolecular Interactions," *The Journal of Chemical Physics* 131 (2009): 014102.

45. T. Bodenstein, A. Heimermann, K. Fink, and C. van Wüllen, "Development and Application of a Complete Active Space Spin-Orbit Configuration Interaction Program Designed for Single Molecule Magnets," *ChemPhysChem* 23 (2022): e202100648.

46. N. F. Chilton, D. Collison, E. J. McInnes, R. E. Winpenny, and A. Soncini, "An Electrostatic Model for the Determination of Magnetic Anisotropy in Dysprosium Complexes," *Nature Communications* 4 (2013): 2551.

47. P. Kalita, J. Goura, J. M. H. Martínez, E. Colacio, and V. Chandrasekhar, "Homodinuclear $\{Ln^{III}_2\}$ (Ln^{III} = Gd^{III}, Tb^{III}, Ho^{III}, and Dy^{III}) Complexes: Field-Induced SMM Behavior of the Dy^{III} and Tb^{III} Analogues," *European Journal of Inorganic Chemistry* 2019 (2019): 212–220.

48. H. Tian, B.-L. Wang, J. Lu, et al., "Consecutive One-/Two-Step Relaxation Transformations of Single-Molecule Magnets *via* Coupling Dinuclear Dysprosium Compounds with Chloride Bridges," *Chemical Communications* 54 (2018): 12105–12108.

49. F. Manna, M. Oggianu, J. R. Galán-Mascarós, et al., "Tuning the Slow Magnetic Relaxation with the Substituents in Anilate Bridged Bis(dysprosium) Complexes," *Dalton Transactions* 53 (2024): 8369–8381.

50. L. Ungur and L. F. Chibotaru, "Magnetic Anisotropy in the Excited States of Low Symmetry Lanthanide Complexes," *Physical Chemistry Chemical Physics* 13 (2011): 20086–20090.

51. Y. C. Chen, J. L. Liu, L. Ungur, et al., "Symmetry-Supported Magnetic Blocking at 20 K in Pentagonal Bipyramidal Dy(III) Single-Ion Magnets," *Journal of the American Chemical Society* 138 (2016): 2829–2837.

52. G. M. Sheldrick, "*SHELXT* – Integrated Space-Group and Crystal-Structure Determination," *Acta Crystallographica Section A Foundations and Advances* 71 (2015): 3–8.

53. G. M. Sheldrick, "Crystal Structure Refinement with *SHELXL*," *Acta Crystallographica Section C Structural Chemistry* 71 (2015): 3–8.

54. O. V. Dolomanov, L. J. Bourhis, R. J. Gildea, J. A. K. Howard, and H. Puschmann, "*OLEX2* : A Complete Structure Solution, Refinement and Analysis Program," *Journal of Applied Crystallography* 42 (2009): 339–341.

Supporting Information

Additional supporting information can be found online in the Supporting Information section.